Microcoils on Structured Silicon Substrates for Magnetic Resonance Detection

Yan Li, Munir M. Ahmad, Jeff W. Hand, Richard R. A. Syms, David Gilderdale, David J. Collins, and Ian R. Young

Abstract—The design and performance of a silicon-based RF detector coil for use in magnetic resonance (MR) spectroscopy applications is described. The coil is fabricated using microelectromechanical systems (MEMS) technology by deep reactive ion etching (DRIE) of an oxidized silicon substrate carrying electroplated conductors. The DRIE step simultaneously forms a sample trough and creates a trepan cut around the coil so that it may be detached from the substrate by cleaving short sections of sprue. A single-turn coil with Q-factor $\sim$16 at 63.6 MHz is demonstrated and MR spectroscopy experiments are described. An accurate numerical model based on the time-domain finite integration technique is used to investigate the effect on the Q-factor of deliberately structuring the substrate to limit the volume of silicon exposed to RF energy. The model is compared with known analytic approximations, and good agreement is obtained.

Index Terms—Magnetic resonance (MR) receiver coils, microcoils, microelectromechanical systems (MEMS), numerical modeling.

I. INTRODUCTION

RECENT WORK HAS suggested that magnetic resonance (MR) spectroscopy may be useful in evaluating cancerous lesions [1], [2]. To obtain data sufficiently quickly, small coils are required to ensure close sample-detector coupling. Since a resonant detector with a high Q-value is required to maximize the signal-to-noise ratio (SNR), one goal is to minimize coil resistivity and leakage. A second goal is the availability of cheap, single-use coils that will avoid potential contamination between patients.

Increasingly, coils are being constructed using microelectromechanical systems (MEMS) technology, thereby allowing

Y. Li is with the Imaging Sciences Department, Clinical Sciences Division, Imperial College London, London W12 0NN, U.K. (e-mail: yan.li3@csc.mrc.ac.uk).

M. M. Ahmad, R. R. A. Syms, D. Gilderdale, and I. R. Young are with the Optical and Semiconductor Devices Group, Department of Electrical and Electronic Engineering, Imperial College London, London SW7 2BT, U.K. (e-mail: m.m.ahmad@imperial.ac.uk; r.syms@imperial.ac.uk; dave.gilderdale@tiscali.co.uk; youngimarl@aol.com).

J. W. Hand is with the Imaging Sciences Department, Clinical Sciences Division, Imperial College London, London W12 0NN, U.K.. He is also with the Radiological Sciences Unit, The Hammersmith Hospitals NHS Trust, London W12 0HS, U.K. (e-mail: j.hand@imperial.ac.uk).

D. J. Collins is with the Cancer Research U.K. Magnetic Resonance Research Group, Institute of Cancer Research and the Royal Marsden NHS Trust, Sutton, Surrey SM2 5PT, U.K. (e-mail: David.Collins@icr.ac.uk).

Digital Object Identifier 10.1109/JSEN.2007.905044

the fabrication of disposable devices with complex, three-dimensional geometries. Planar spiral microcoils fabricated by lithography and electroplating [3], and solenoidal microcoils constructed by methods including nonplanar lithography, multilayer lithography and self-assembly [4]–[6], have been reported. MR detector coils have been combined with etched troughs to increase coupling to the sample [7], Q-factors have been increased on glass substrates [8], capacitors [9] and transistors [10] have been integrated on-chip and implantable coils have been developed [11]. Helmholtz coils, which offer increased field uniformity, have also been constructed from stacked substrates [12], [13].

One of the most interesting approaches to microcoil construction is silicon MEMS, since this allows the substrate to be structured accurately into arbitrary shapes such as sample troughs [14] and needles [15] by deep reactive ion etching (DRIE). However, the presence of a nearby semiconducting substrate degrades the Q-factor, an effect well known in silicon integrated circuit design [16]–[18]. Despite this, empirical methods have been used to develop silicon-based microcoils for MRS using intrinsic substrates with thick oxide isolation that have Q-factors as high as 25 at 200 MHz [14] and can, therefore, detect useful spectral data [15]. The high sensitivity of Q-factor to local loss mechanisms, and the fact that the topography of MRS detector coils differs from the uniform silicon substrate of a simple integrated inductor in an ultra large-scale integration (ULSI) circuit, give rise to the need for accurate models as part of the design process.

In this paper, we describe construction of experimental microcoils using metal electroplating and DRIE of silicon substrates, and present typical experimental results, including initial MR spectroscopy experiments. An equivalent circuit model and a numerical approach are used to explore the effect of varying different design parameters of structured substrates and to demonstrate the beneficial effect of removal of silicon from key regions around the coil.

II. MICROCOIL FABRICATION

Experimental microcoils were constructed using the process outlined in Fig. 1(a) [14]. 100 mm diameter, $\langle 100 \rangle$-oriented, intrinsic Si-wafers of resistivity 5 kΩm were thermally oxidized to form a 1 μm thick isolation layer. The resistivity of the Si-wafers measured after stripping the thermally grown oxide was found to be 50 Ωm. This was considered to be due to a combination of surface contamination during thermal oxidation and interface states [19]. A conductive seed layer of 300 Å Ti and 2000 Å Cu metal was then deposited by RF sputter-coating. Next, a 22 μm thick layer of AZ9260 photoresist was spin-
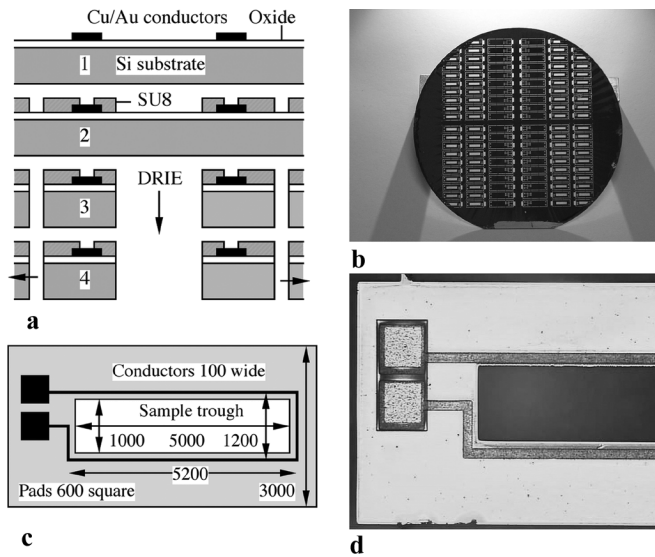
Fig. 1. (a) Fabrication process for silicon-based microcoils. (b) Completed wafer. (c) Die layout. (d) Completed device die.

Fig. 2. Schematic diagrams showing location of samples in two MR experiments. (a) Spenco sample. (b) Cod liver oil sample.

coated and patterned to provide a mould for electroplating. Conductors were formed using 14 μm Cu and 4 μm Au, which were both plated using commercial solutions (Technic FB, from Lektrachem, and ECF 60, from Metalor, respectively). The mould was then stripped, together with residual areas of exposed seed metal. The wafer was then coated with a 20 μm thick layer of AZ9260 photoresist. Using this layer as a mask, the oxide layer and then the wafer were etched through completely by DRIE, a method of near vertical etching that operates by cyclic etching and passivation of silicon using a high-density inductively coupled plasma. Fig. 1(b) shows a wafer after completion of processing.

Detectors were formed as single-turn coils based on a 100 μm wide conductor surrounding an etched sample trough measuring 5 mm $\times$ 1 mm, as shown in Fig. 1(c). The coils were attached to the wafer using short sections of silicon sprue, which could be cleaved to detach the dies without the need for dicing. A completed device die is shown in Fig. 1(d).

Electrical connections to a silicon baseplate were formed using indium metal as solder. Coil assemblies were configured as parallel resonators using surface mount capacitors. Coil performance was measured using an Agilent E5061A vector network analyser. Four-point probe measurements of wafers stripped of thermal oxide were also carried out.

III. MR EXPERIMENTS

MR experiments were performed using a 1.5 T Siemens Magnetron Vision system. The Vision system body coil was used for RF transmission and a microcoil, placed within a body coil loading annulus, was used as the signal receiver. A free induction decay was obtained using the following measurement parameters, repetition time (TR) 2.0 s, nonselective 500 μs excitation pulse (90°), two averages and receiver gain set at 90 dB. Data processing comprised of FFT and manual phase correction.

Two experiments were carried out. In one, the microcoil was loaded with a sample of Spenco, a vinyl plastisol material (Spenco Healthcare International, Horsham, U.K.), measuring
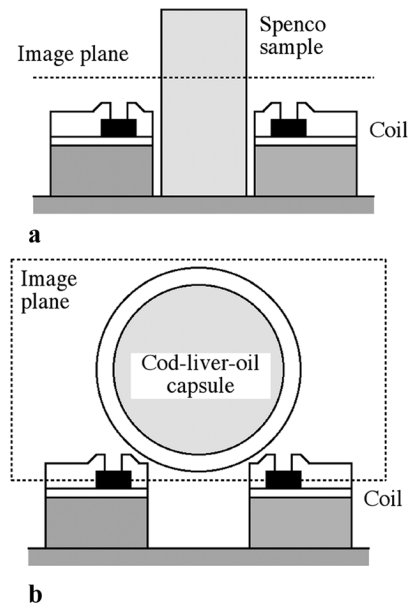
4 mm $\times$ 0.7 mm $\times$ 0.7 mm, and standing vertically on its long edge within the sample volume of the coil [Fig. 2(a)], which provided a source of mobile protons. Unlike other sources of protons such as doped water or oils, Spenco is stable over a period of several years and does not exhibit evaporation and/or leakage with time. It can also be easily moulded, an important factor when minimizing susceptibility disturbances at sample interfaces. A disadvantage of Spenco is that its relaxation properties are not ideal since the material is semiplastic with relatively broad intrinsic linewidth. However, overall, Spenco has proven to be a useful signal source [20].

In the second experiment, a semicylindrical capsule of cod liver oil, approximately 10 mm in height and 8 mm in diameter, was placed directly above the microcoil [Fig. 2(b)].

IV. NUMERICAL MODEL

Numerical modeling was carried out using a commercial electromagnetic, time-domain solver within CST Microwave Studio V 5.1.3 and V 2006 (Computer Simulation Technology, Darmstadt, Germany). This provides a solution to the time-dependent Maxwell's equations using a time-domain variant of the Finite Integration Technique (FIT) [20]. A summary of the method is given in [22].

Fig. 3 shows the geometry of the model consisting of a rectangular silicon substrate mounting a single-turn conductor on an insulating spacer. The dimensions, similar to those in the experimental device, are listed in Table I and material properties used are given in Table II. An open boundary condition with added space was used and the model was meshed to a hexahedral grid. The minimum and maximum mesh steps used were 1 μm and 693 μm, respectively; the total number of mesh cells was >4 million. The coil was excited by a Gaussian voltage pulse of 888.6 ps duration applied across the left ends of the copper conductors. Time stepping with an increment as small as 1.9 fs was necessary because of the fine mesh. The impedance was found
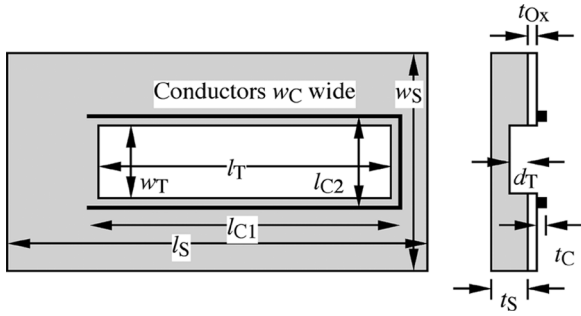
Fig. 3. Model of single-turn coil.

TABLE I
DIMENSIONS USED IN THE NUMERICAL AND
EQUIVALENT CIRCUIT MODELS

Parameter		Dimension
		(μm)
l_S	substrate length	8200
w_S	substrate width	3000
t_S	substrate thickness	535
t_{Ox}	insulating layer thickness	1
t_C	copper track thickness	14
l_{C1}	length of long copper track	5250
l_{C2}	length of short copper track	1200
w_C	copper track width	100
Trough (where appropriate)		
w_T	width of trough	1100
l_T	length of trough	5200
d_T	depth of trough	0 - 500

TABLE II
MATERIAL PROPERTIES USED IN THE NUMERICAL AND
EQUIVALENT CIRCUIT MODELS

Material	Relative permittivity ε_r	Conductivity σ (S m^{-1})	Permeability μ (H m^{-1})
Silicon (Si)	11.9 (ε_{Si})	0.02 (σ_{Si})	$4\pi \times 10^{-7}$
Silica (SiO$_2$)	3.97 (ε_{Ox})	3.33×10^{-16} (σ_{Ox})	$4\pi \times 10^{-7}$
Copper (Cu)	1	5.8×10^7 (σ_{Cu})	$4\pi \times 10^{-7}$

from the S-parameter S_{11} and the dependence of Q-factor on frequency from $Q = X/R$, where X and R are the reactance and resistance, respectively. The model ran on a Pentium 4 CPU 3.73 GHz PC with 4 GB of RAM and the typical total solver time was approximately 24 days. This was because of the very small minimum cell size, the overall size of the model, and the relatively low frequency used in this time-domain technique. The runtime was sufficiently long as to eliminate blind variation as a possibility of exploring parameter space.
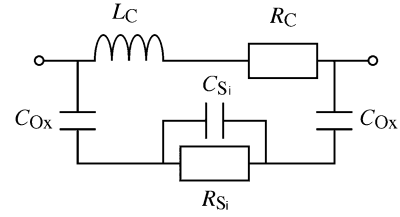
Fig. 4. Equivalent circuit of single-turn coil.

V. EQUIVALENT CIRCUIT MODEL

To allow appropriate parameters to be identified more quickly, an equivalent circuit representing a single-turn coil on a uniform substrate was developed, as shown in Fig. 4. The inductance and resistance of the conductor are represented by L_C and R_C. C_{Ox}, C_{Si}, and R_{Si} represent the oxide capacitance, the silicon substrate capacitance, and the silicon substrate resistance, respectively. Since the distance between the two parallel conductors is relatively large in the present case ($\sim 1200 \ \mu m$), the effect of capacitive coupling between the input and output ports of the coil is negligible. The separation between the two parallel conducting tracks is also sufficiently large for the proximity effect of one copper conductor on the other to be ignored. Eddy currents induced in the substrate are ignored too since the conductivity of the substrate and the working frequency are both relatively low. The skin effect is considered in this lumped element model.

The input impedance associated with the equivalent circuit is

$$Z = \cfrac{1}{\cfrac{1}{1/(j\omega C_{Si}+1/R_{Si})+2/(j\omega C_{Ox})} + \cfrac{1}{R_C + j\omega L_C}} \qquad (1)$$

where ω is the angular frequency. The inductance L_C is comprised of self inductance and mutual inductance components and is given (in nH) by [23]

$$L_C = 0.4 l_{C1}\left[ln\left(\frac{l_{C2}}{w_C + t_C}\right) + 1.5 + A_1 - A_2\right] + 0.2 l_{C2}\left[ln\left(\frac{2l_{C2}}{w_C + t_C}\right) + 0.5 - A_2\right]. \quad (2)$$

The parallel conductors have equal and rectangular cross sections $w_C \times t_C (w_C > t_C)$, and their length l_{C1} is large compared with their separation l_{C2}. All dimensions are in millimeters (mm). A_1 is a constant relating to the distances between the conductors and A_2 is a constant relating to the geometric mean of the conductor cross-sectional dimensions. A_1 and A_2 are determined from tabulated data in [23] and for the present model are -0.006 and 0.0023, respectively. Using (2), L_C is found to be approximately 9 nH.

At high frequency, a thick conductor supports a current density that decays exponentially from the surface to the center of the conductor. If the thickness of the conductor t_C is comparable to the skin depth δ, an effective one dimensional skin depth [24] is given by

$$\delta_{\text{eff}} = \delta\left[1 - \exp(-t_C/\delta)\right] \qquad (3)$$

where $\delta = \sqrt{1/(\pi\sigma\mu f)}$ and σ, μ, and f are the conductivity (S m^{-1}) and the permeability (H m^{-1}) of the conductor, and

the frequency (Hz), respectively. For copper, $\sigma_{\mathrm{Cu}} = 5.8 \times 10^7$ S m^{-1} and $\delta \sim 8$ μm when the frequency is 64 MHz. The series resistance, R_{C}, can be expressed as

$$R_{\mathrm{C}} = \frac{l_{\mathrm{C}}}{\sigma_{\mathrm{Cu}} w_{\mathrm{C}} \delta_{\mathrm{eff}}} \qquad (4)$$

where l_{C} represents the total length of the conductor, namely, $l_{\mathrm{C}} = 2l_{\mathrm{C}1} + l_{\mathrm{C}2}$. According to [24] and [25], the capacitance C_{Ox} due to the SiO$_2$ layer may be found using

$$\begin{aligned}
C_{\mathrm{Ox}} = \varepsilon_{\mathrm{Ox}} \varepsilon_0 & \left(l_{\mathrm{C}1} + \frac{l_{\mathrm{C}2}}{2} \right) \\
& \times \Big\{ 1.15 w_{\mathrm{C}}/t_{\mathrm{Ox}} + 2.80 (t_{\mathrm{C}}/t_{\mathrm{Ox}})^{0.222} \\
& \quad \times \left[1 + w_{\mathrm{C}} \Big/ \left(l_{\mathrm{C}1} + \frac{l_{\mathrm{C}2}}{2} \right) \right] + 4.12 (t_{\mathrm{C}}/t_{\mathrm{Ox}})^{0.728} \\
& \quad \times \left[t_{\mathrm{Ox}} \Big/ \left(l_{\mathrm{C}1} + \frac{l_{\mathrm{C}2}}{2} \right) \right] \Big\}
\end{aligned} \qquad (5)$$

where ε_0 is the permittivity of free space. The resistance R_{Si} of the silicon substrate is calculated using [26]

$$R_{\mathrm{Si}} \approx \frac{\ln 2 + 2 \tanh^{-1} \sqrt{k}}{\sigma_{\mathrm{Si}} \pi} \qquad (6)$$

where $k = \sqrt{1 - (w_{\mathrm{C}}/l_{\mathrm{C}2})^2}$ and the capacitance C_{Si} of the silicon substrate can be obtained from the relaxation time constant $\varepsilon_{\mathrm{Si}} \varepsilon_0 / \sigma_{\mathrm{Si}}$ [27] as

$$C_{\mathrm{Si}} = \frac{\varepsilon_{\mathrm{Si}} \varepsilon_0}{\sigma_{\mathrm{Si}} R_{\mathrm{Si}}}. \qquad (7)$$

The impedance and Q-factor are found using a Matlab program employing the above parameters and equations.

VI. RESULTS

A. Electrical Performance of Microcoil

Typical DC values of inductance and series resistance were 11.2 nH and 0.15 Ω, respectively. Using (2), L_{C} is found to be approximately 9 nH, slightly below the experimental value due to the omission of short track segments leading to the bond pads.

Fig. 5 shows a typical variation of Q-factor with frequency. At low frequencies, the Q-factor rises linearly, but at intermediate frequencies, the rate of increase slows and the Q-factor peaks at ≈ 23 at approximately 150 MHz. This performance is worse than expected from devices fabricated on intrinsic Si, which should approach that achievable on glass. Four-point probe measurements of wafers stripped of thermal oxide revealed a decrease in resistivity to around 0.5 Ωm.

Fig. 6 shows the frequency dependence of impedance of a single turn, resonant detector tuned to 63.87 MHz (the proton resonance frequency in a 1.5 T field).

B. MR Performance of Microcoil

Preliminary results regarding MR spectra obtained from the Spenco and cod liver oil samples are shown in Fig. 7(a) and (b), respectively. Linewidths are full width at half maximum unless
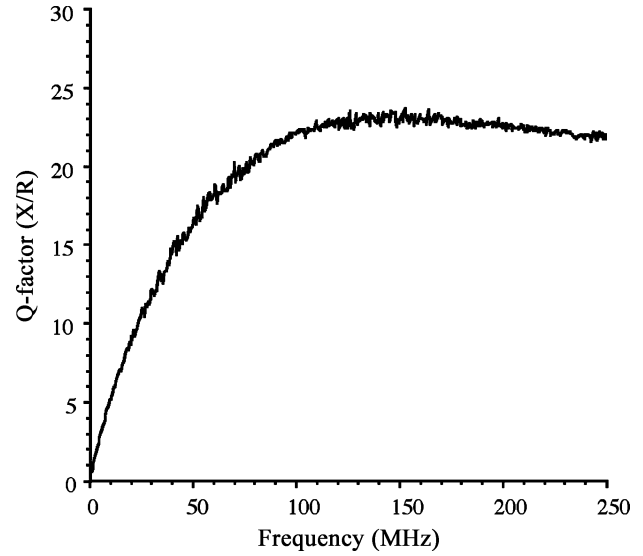
Fig. 5. Experimental variation of Q-factor with frequency for single-turn coil.
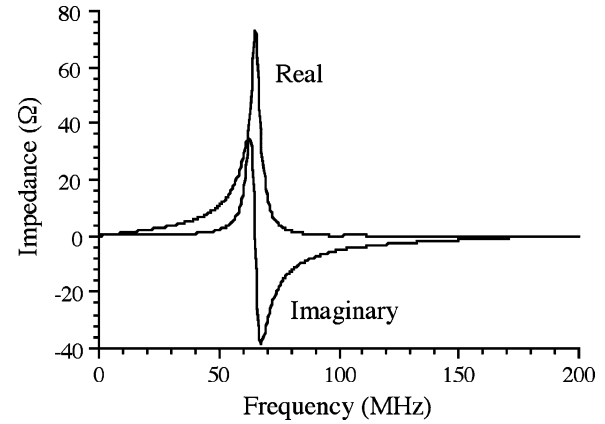
Fig. 6. Experimental variation of impedance with frequency for resonant single-turn coil.

explicitly stated otherwise. The Spenco spectrum exhibited a large peak, approximately 54 Hz wide, and two clearly resolved side peaks. Spenco is semiplastic, and therefore has a relatively broad intrinsic linewidth. The sample is also small and, therefore, the environment includes air/Spenco and other interfaces that will contribute further to line broadening through slightly different susceptibilities. The spectrum from the cod liver oil sample showed the linewidth of the lipid peak to be 12–17 Hz. The SNR, estimated to be approximately 900, was obtained from two averages and so assuming Gaussian noise, the SNR per acquisition was $900/\sqrt{2}$. The B1 field varied from 100% (at the edge of the sample adjacent to coil based on the image data from the cod liver oil) to approximately 10% over 2.4 mm.

The data shown here have been apodized to boost high frequencies; this procedure helps to identify doublets, which can, otherwise, appear as a single broad peak. Considerable structure may be seen in the oil spectrum, and preliminary assignment of the different peaks is in progress. Unlike the Spenco sample which was comparable in size to the coil components, the oil sample was relatively large and any local effects would be masked by the signal from the large sample volume.
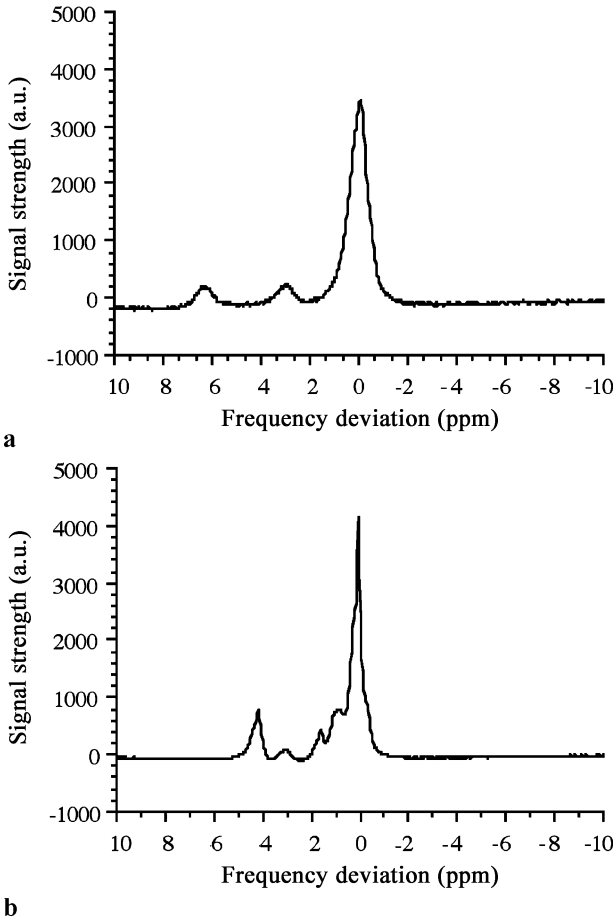
Fig. 7. MR spectra obtained using a single-turn coil. (a) "Spenco" sample. (b) Cod liver oil capsule.
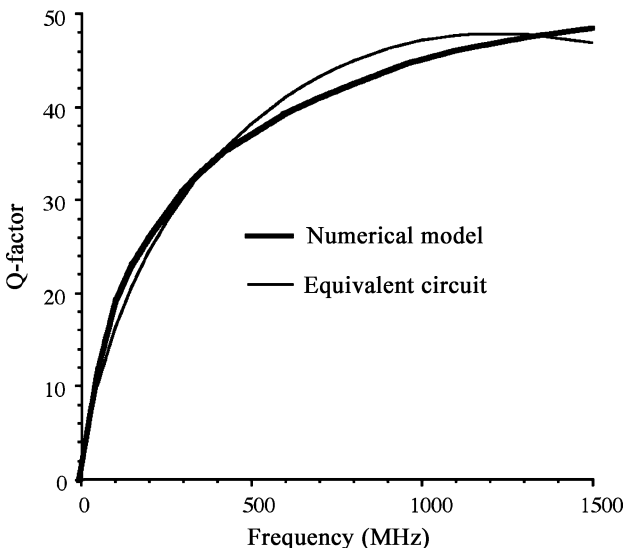
Fig. 8. Frequency dependence of Q-factor predicted by the equivalent circuit and numerical models.

C. Comparison Between Numerical and Equivalent Circuit Models

1) Frequency Dependence of Q: Fig. 8 shows the frequency dependence of the Q-factor as predicted by each model. The two agree extremely well over the wide frequency range shown. However, agreement with the experiment is surprisingly poor;

both theoretical models predict peak Q-factors that are much higher than the experimental device, and occur at much higher frequencies. We explore possible explanations below.

2) Substrate Resistivity: Given the results of the four-point probe test, it is natural to investigate the effect of limited substrate resistivity. Fig. 9(a) shows the variations of Q-factor with frequency predicted using the equivalent circuit when the resistivity $\rho_{Si} = 1/\sigma_{Si}$ was varied. The thickness of the SiO_2 insulating layer was kept fixed at 1 μm. In general, the trend is for both the maximum Q-factor and the frequency at which it occurs to decrease with decreasing resistivity. However, when $\rho_{Si} < 0.1$ Ωm, a small increase in the maximum value and the corresponding frequency is predicted as the resistivity is decreased. The maximum Q-factor for $\rho_{Si} = 0.5$ Ωm is somewhat below the experimental result.

3) Isolation Layer Thickness: Fig. 9(b) shows the variation of Q-factor with frequency predicted using the equivalent circuit model assuming now that the thickness of the SiO_2 layer is varied from 1 to 100 μm. The resistivity was 0.5 Ωm. Although it is difficult to form a SiO_2 layer thicker than 4 μm by thermal oxidation, thicknesses in the range studied are possible using SU-8, which has a similar permittivity to SiO_2 and a very high-resistivity ($\approx 10^{14}$ Ωm). Although SU-8 contains protons, this would not be problematic in MR applications since a significant signal would not be obtained without the specialized techniques of solid-state MR. The results suggest that the maximum Q-factor rises, together with the corresponding frequency, as the insulator thickness increases. However, unrealistically large thicknesses are required to obtain a Q-factor similar to the experiment.

4) Silicon Structuring: We now consider the effect of structuring the silicon itself, first into a die of finite size. These possibilities are simulated using the numerical model. Fig. 10(a) shows the predicted variation of Q-factor with frequency for cases in which the substrate dimensions are varied, following the pattern $l_S \approx N \times l_{C1}$ and $w_S \approx N \times l_{C2}$, where N is a constant multiplier. In each case, a substrate resistivity of 0.5 Ωm and an oxide thickness of 1 μm are assumed. The other dimensions and material properties are as in Tables I and II. The results suggest that the maximum Q-factor and the associated frequency increase as the substrate dimensions tend to those of the coil itself. Removal of lossy surrounding material clearly allows improved performance without the need for an unrealistic isolation layer thickness.

We now consider the effect of an etched cuboid sample trough cut through the isolation layer and the silicon, whose perimeter lies just inside the coil. Fig. 10(b) shows the predicted variation of Q-factor with frequency, for various trough depths d_T. The parameters assumed are as in Table I. The results imply that performance improves as the trough is made deeper, and the peak Q-factor now approaches the experimental result for the deepest etch.

VII. DISCUSSION

The results above suggest that optimum performance is achieved when the resistivity of the silicon substrate is maximized, the thickness of the insulating layer is maximized, the dimensions of the substrate are minimized and the volume of
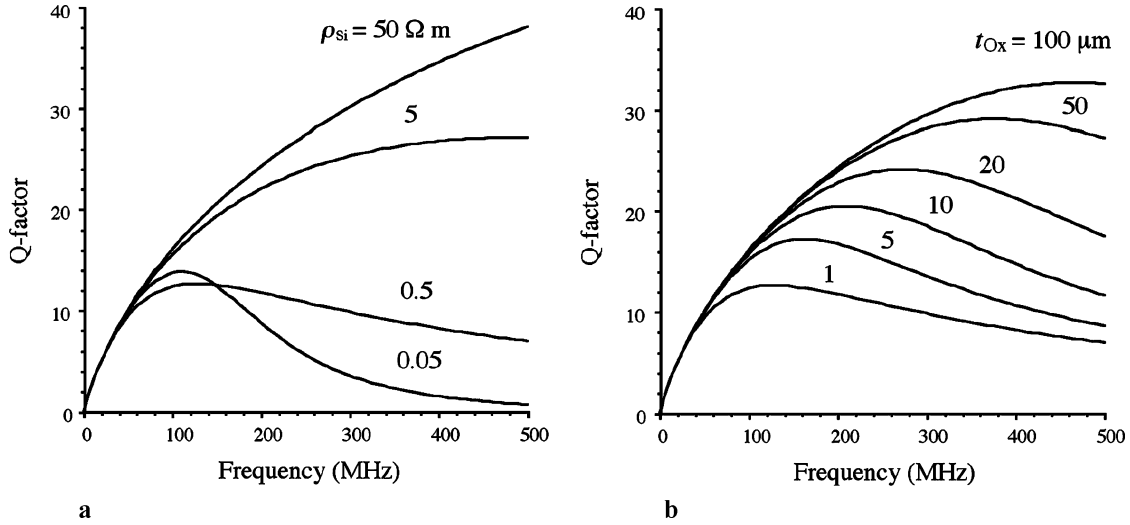
Fig. 9. Frequency dependence of Q-factor predicted by the equivalent circuit model. (a) For different substrate resistivities ρ_{Si} and a fixed oxide thickness of $t_{\mathrm{Ox}} = 1 \, \mu\mathrm{m}$. (b) For different oxide thicknesses t_{Ox} and a fixed substrate resistivity $\rho_{\mathrm{Si}} = 0.5 \, \Omega\mathrm{m}$.
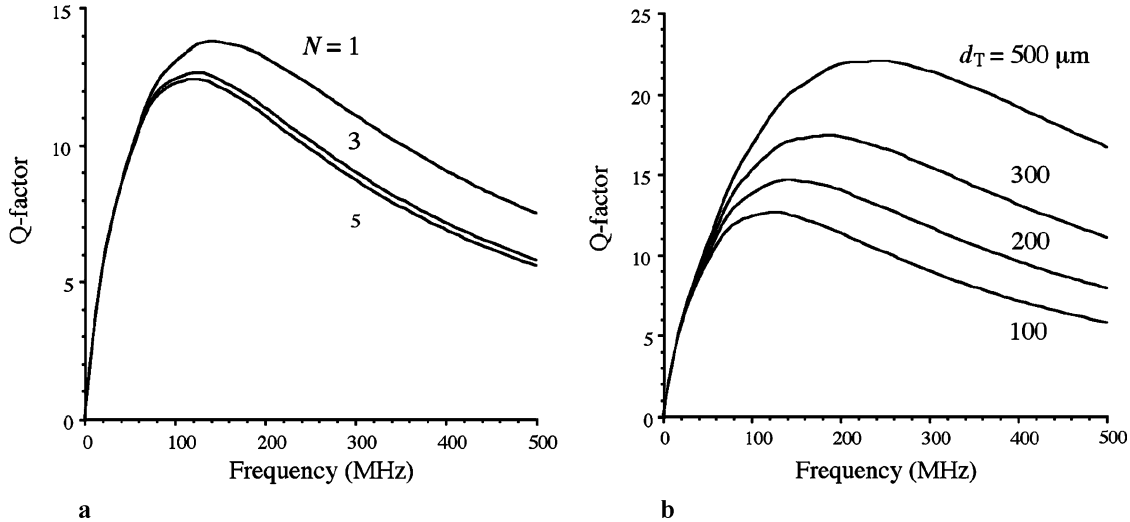
Fig. 10. Frequency dependence of Q-factor predicted by the numerical model. (a) For different relative substrate sizes N. (b) For different sample trough depths d_{T}.

the sample trough is maximized. It is worthwhile considering the physical reasons for this behavior.

When the substrate resistivity is increased beyond $\approx 0.1 \, \Omega\mathrm{m}$, the resistance of the substrate increases, energy loss in the substrate is decreased, and the Q value increases, as shown in Fig. 9(a). As the resistivity continues to increase, the substrate branch of the equivalent circuit shown in Fig. 4 (i.e., C_{Ox}, R_{Si}, and C_{Si}) approaches an open circuit condition and the frequency associated with the maximum Q-factor increases. However, more complex behavior occurs when the substrate resistivity is low, as we now show.

The impedance of the substrate branch Z_{sub} is

$$Z_{\mathrm{sub}} = \frac{1}{j\omega C_{\mathrm{Si}} + \frac{1}{R_{\mathrm{Si}}}} + \frac{2}{j\omega C_{\mathrm{Ox}}}$$
$$= \frac{\omega R_{\mathrm{Si}} C_{\mathrm{Ox}} - j\left(\omega^2 R_{\mathrm{Si}}^2 C_{\mathrm{Si}} C_{\mathrm{Ox}} + 2 + 2\omega^2 R_{\mathrm{Si}}^2 C_{\mathrm{Si}}^2\right)}{\omega C_{\mathrm{Ox}}\left(1 + \omega^2 R_{\mathrm{Si}}^2 C_{\mathrm{Si}}^2\right)} \quad (8)$$

and the corresponding Q-factor Q_{sub} is

$$Q_{\mathrm{sub}} = -\frac{\omega^2 R_{\mathrm{Si}}^2 C_{\mathrm{Si}}(C_{\mathrm{Ox}} + 2C_{\mathrm{Si}}) + 2}{\omega R_{\mathrm{Si}} C_{\mathrm{Ox}}}. \quad (9)$$

At low angular frequencies, such that $\omega^2 \ll \omega_c^2$, where $\omega_c^2 = 2/(R_{\mathrm{Si}}^2 C_{\mathrm{Si}}(C_{\mathrm{Ox}} + 2C_{\mathrm{Si}}))$, then $|Q_{\mathrm{sub}}| \approx 2/(\omega R_{\mathrm{Si}} C_{\mathrm{Ox}})$. Under these conditions, $|Q_{\mathrm{sub}}|$ increases when ρ_{Si} and R_{Si} decrease. However, when $\omega^2 \gg \omega_c^2$, $|Q_{\mathrm{sub}}| \approx \{\omega R_{\mathrm{Si}} C_{\mathrm{Si}}(C_{\mathrm{Ox}} + 2C_{\mathrm{Si}})\}/C_{\mathrm{Ox}}$, and the opposite occurs. By differentiating, we can show that the maximum is at $\omega = \sqrt{2/[C_{\mathrm{Si}}(C_{\mathrm{Ox}} + 2C_{\mathrm{Si}})]}/R_{\mathrm{Si}}$. On the other hand, for the conductor branch of the equivalent circuit, the Q-factor is $Q_{\mathrm{cond}} = \omega L_{\mathrm{C}}/R_{\mathrm{C}}$, where L_{C} and R_{C} are as given in (2) and (4). As a result, Q_{cond} increases with increasing frequency.

The net effect is that at low frequencies, conductor effects dominate—Q increases with increasing frequency, and the substrate resistivity has little effect. At high frequencies, the sub-

strate plays an increasing role and the coil eventually becomes capacitive. Clearly, if the substrate resistivity is limited, it is important to compensate as far as possible by structuring the substrate to remove the maximum unnecessary material.

VIII. CONCLUSION

We have demonstrated a wafer-scale process for batch fabrication of MR detectors on oxidized silicon substrates. The conductors are formed first, by electroplating metals inside a photoresist mould, and the die topography is then defined by DRIE.

Good electrical performance has been demonstrated, with Q-factors up to 15, despite the use of a semiconducting substrate. Preliminary MRS experiments have been performed, and good SNR and linewidth have been obtained. This level of performance is extremely encouraging, and confirms the essential validity of the fabrication scheme. However, further improvements in signal obtained from optimized multiturn coil geometries and from an increase in magnetic field strength (and hence in operating frequency) are expected. Use of microcoils in evaluating tissue samples is in progress.

It has also been shown that reasonable Q-factors can be achieved using high-resistivity silicon substrates, selective substrate removal both inside and outside the coil, and thick oxide isolation layers. By accounting for these factors, experimental performance of microcoils has been verified using a detailed numerical model, with additional physical insight being provided by a simple equivalent circuit.

REFERENCES

[1] T. Tamiya, K. Kinoshita, Y. Ono, K. Matsumoto, T. Furuta, and T. Ohmoto, "Proton magnetic resonance spectroscopy reflects cellular proliferative activity in astrocytomas," *Neuroradiology*, vol. 42, pp. 333–338, May 2000.

[2] S. J. Barton, F. A. Howe, A. M. Tomlins, S. A. Cudlip, J. K. Nicholson, B. A. Bell, and J. R. Griffiths, "Comparison of in vivo ^{1}H MRS of human brain tumours with ^{1}H HR-MAS spectroscopy of intact biopsy samples in vitro," *MAGMA*, vol. 8, pp. 121–128, May 1999.

[3] T. L. Peck, R. L. Magin, and P. C. Lauterbur, "Design and analysis of microcoils for NMR microscopy," *J. Magn. Reson. B*, vol. 108, pp. 114–124, Aug. 1995.

[4] J. A. Rogers, R. J. Jackman, G. M. Whitesides, D. L. Olson, and J. V. Sweedler, "Using microcontact printing to fabricate microcoils on capillaries for high resolution proton nuclear magnetic resonance on nanoliter volumes," *Appl. Phys. Lett.*, vol. 70, pp. 2464–2466, May 1997.

[5] C. H. Ahn and M. G. , "Micromachined planar inductors on silicon wafers for MEMS applications," *IEEE Trans. Ind. Electron.*, vol. 45, pp. 866–876, Dec. 1998.

[6] J.-B. Yoon, B.-K. Kim, C.-H. Han, E. Yoon, and C.-K. Kim, "Surface micromachined solenoid on-Si and on-glass inductors for RF applications," *IEEE Electron Device Letts.*, vol. 20, pp. 487–489, Sep. 1999.

[7] J. Dechow, A. Forchel, T. Lanz, and A. Haase, "Fabrication of NMR-microsensors for nanoliter sample volumes," *Microelectr. Eng.*, vol. 53, pp. 517–519, June 2000.

[8] C. Massin, C. Boero, F. Vincent, J. Abenhaim, P. A. Besse, and R. S. Popovic, "High-Q factor RF planar microcoils for micro-scale NMR spectroscopy," *Sens. Actuators A*, vol. 97–98, pp. 280–288, Apr. 2002.

[9] D. Ellersiek, S. Harms, F. Casanova, B. Blümich, W. Mokwa, and U. Schnakenberg, "Flexible RF microcoils with integrated capacitor for NMR applications," in *Proc 16th Workshop on Micromach., Micromech., Microsyst.*, Göteborg, Sweden, Sep. 5–6, 2005, pp. 256–259.

[10] J. Dechow, T. Lanz, M. Stumber, A. Forchel, and A. Haase, "Preamplified planar microcoil on GaAs substrates for microspectroscopy," *Rev. Sci. Instrum.*, vol. 74, pp. 4855–4857, Nov. 2003.

[11] L. Renaud, M. Armenean, L. Berry, P. Kleimann, P. Morin, M. Pitaval, J. O'Brien, M. Brunet, and H. Saint-Jalmes, "Implantable planar rf microcoils for NMR microspectroscopy," *Sens. Actuators A*, vol. 99, pp. 244–248, Jun. 2002.

[12] J. H. Walton, J. S. de Ropp, M. V. Shutov, A. G. Goloshevsky, M. J. McCarthy, R. L. Smith, and S. D. Collins, "A micromachined double-tuned NMR microprobe," *Anal. Chem.*, vol. 75, pp. 5030–5036, Oct. 2003.

[13] R. R. A. Syms, M. M. Ahmad, I. R. Young, Y. Li, J. Hand, and D. Gilderdale, "MEMS Helmholtz coils for magnetic resonance imaging," *J. Micromech. Microeng.*, vol. 15, pp. S1–S9, Jul. 2005.

[14] R. R. A. Syms, M. M. Ahmad, I. R. Young, D. Gilderdale, D. J. Collins, and M. O. Leach, "Batch fabrication of micro-coils for MR spectroscopy on silicon," in *Proc 4th IEEE. Conf. Sensors*, Irvine, CA, Oct. 31–Nov. 1 2005, pp. 227–230.

[15] F. A. Howe, J. R. Griffiths, L. Rodrigues, R. R. A. Syms, M. M. Ahmad, and I. R. Young, " ^{31}P spectroscopy using a silicon-based needle coil," in *Proc 14th Annu. Meeting of ISMRM Scientific Meeting*, Seattle, WA, May 6–12, 2006, p. 3101.

[16] J. Gil and H. Shin, "A simple wide-band on-chip inductor model for silicon-based RF ICs," *IEEE Trans. Microwave Theory Tech.*, vol. 51, pp. 2023–2027, Sep. 2003.

[17] T. Pan, A. Baldi, E. Davies-Venn, R. F. Drayton, and B. Ziaie, "Fabrication and modelling of silicon-embedded high-Q inductors," *J. Micromech. Microeng.*, vol. 15, pp. 849–854, Apr. 2005.

[18] A. M. Hynes, H. Ashraf, J. K. Bhardwaj, J. Hopkins, I. Johnston, and J. N. Shepherd, "Recent advances in silicon etching for MEMS using the ASE process," *Sens. Actuators A*, vol. 74, pp. 13–17, Apr. 1999.

[19] J. F. Zhang, P. Watkinson, S. Taylor, and W. Eccleston, "Interface state behaviour of plasma grown oxides following low temperature annealing," *Appl. Surface Sci.*, vol. 39, pp. 374–380, Oct. 1989.

[20] D. J. Herlihy, D. J. Larkman, N. M. deSouza, A. D. Williams, and I. R. Young, "Catheter tracking for MR fluoroscopy: Design of a transmit/receive coil for use with a nasogastric tube," *J. Magn. Reson. Imag.*, vol. 13, pp. 127–130, Jan. 2001.

[21] T. A. Weiland, "Time domain electromagnetic field computation with finite difference methods," *Int. J. Num. Modeling: Electronic Networks, Devices and Fields*, vol. 9, pp. 295–319, Jul. 1996.

[22] J. W. Hand, Y. Li, E. L. Thomas, M. A. Rutherford, and J. V. Hajnal, "Prediction of specific absorption rate in mother and fetus associated with MRI examinations during pregnancy," *Mag. Reson. Med.*, vol. 44, pp. 883–893, Apr. 2006.

[23] F. W. Grover, *Inductance Calculations, Working Formulas and Tables.* New York: Instrument Society of America, 1973.

[24] Y. Eo and W. R. Eisenstadt, "High-speed VLSI interconnect modeling based on S-parameter measurements," *IEEE Trans. Compon., Hybrids, Manuf. Technol.*, vol. 6, pp. 555–562, Aug. 1993.

[25] T. Sakurai and K. Tamaru, "Simple formula for two- and three- dimensional capacitances," *IEEE Trans. Electron Devices*, vol. 30, pp. 183–185, Feb. 1983.

[26] H. Grabinski, B. Konrad, and P. Nordholz, "Simple formulas to calculate the line parameters of interconnects on conducting substrates," in *Proc IEEE 7th Topical Meeting on Electrical Performance of Electronic Packaging*, West Point, NY, Oct. 26–28, 1998, pp. 223–226.

[27] A. Luoh and A. Weisshaar, "Closed-form expressions for the line parameters of co-planar on-chip interconnects on lossy silicon substrates," in *Proc IEEE 11th Topical Meeting on Electrical Performance of Electronic Packaging*, Monterey, CA, Oct. 21–23, 2002, pp. 341–344.
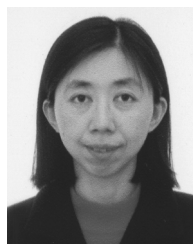
Yan Li received the B.S., M.S., and Ph.D. degrees from the Harbin Institute of Technology, Harbin, China, in 1992, 1995, and 1998, respectively.

She is currently a Research Associate working on numerical simulation of MR devices and MR safety related problems. She has held previous research posts with the Department of Orthopaedics, University of Aberdeen, U.K., the Mechanical Engineering Laboratory, Tsukuba, Japan, and with the Laboratoire de Électronique, Information et Image, Université de Bourgogne, Dijon, France. She has published some 20 peer-reviewed papers in the fields of robotics, electrical discharge machining, and MRI safety.

Munir M. Ahmad received the M.Sc. and Ph.D. degrees in chemistry from the University of Bradford, Bradford, U.K. His Ph.D. dissertation focused on the synthesis, electrical and magnetic properties of organic semiconductors.

He is a Member of Research Staff in the Department of Electrical and Electronics Engineering, Imperial College London. He has worked on a number of projects related to microengineering, microelectromechanical systems, and materials for optical devices. Currently, he is involved in the research and development of MEMS devices for biomedical applications.

Dr. Ahmad is a Chartered Chemist and a Fellow of the Royal Society of Chemistry.

Jeff W. Hand received the B.Sc., Ph.D., and D.Sc. degrees from the University of Newcastle upon Tyne, Newcastle upon Tyne, U.K., in 1967, 1972, and 1995, respectively.

He is Director of the Radiological Sciences Unit, Hammersmith Hospitals NHS Trust, London, and a Professor of Imaging Physics at Imperial College London. He has held research posts at Birkbeck College, University of London, the U.K. Medical Research Council's Cyclotron Unit, London, Stanford University, the University of Arizon, and at Shimane Medical University, Izumo, Japan. He has worked on therapeutic and diagnostic applications of nonionising radiations in medicine, including the modeling of MRI devices and MR safety related problems, for 31 years, and has authored more than 190 scientific papers in journals and books.

Dr. Hand is a Fellow of the Institute of Physics, a Fellow of the Institution of Engineering and Technology, and a Fellow of the Institute of Physics and Engineering in Medicine. He is also a registered Clinical Scientist, a Chartered Engineer, a Chartered Physicist, and a Chartered Scientist. Amongst his professional activities he is currently a member of Council of the Institute of Physics and Engineering in Medicine.

Richard R. A. Syms was born in Norfolk, VA, in 1958. He received the B.A. degree in engineering science and the D.Phil. degree (on volume holographic optical elements) from Worcester College, Oxford, U.K., in 1979 and 1982, respectively.

He has been Head of the Optical and Semiconductor Devices Group in the Department of Electrical and Electronics Engineering, Imperial College London, since 1992 and Professor of Microsystems Technology, since 1996. He has published over 100 journal papers and two books on holography, integrated optics, laser and amplifier devices, and microengineering. He is Co-Founder and Research Director of the MEMS spin-out company Microsaic Systems.

Prof. Syms is a Fellow of the Institute of Electrical Engineers (IEE), the Institute of Physics, and the Royal Academy of Engineering. He is an Associate Editor for the IEEE/ASME JOURNAL OF MICROELECTROMECHANICAL SYSTEMS.

David Gilderdale photograph and biography not available at the time of publication.

David J. Collins is a Principal Clinical Scientist with the Cancer Research United Kingdom (CRUK) Clinical Magnetic Resonance Research Group, Royal Marsden Hospital, Sutton U.K. Having originally trained in electrical engineering and physics, he moved on to medical physics research in 1986 at the Royal Marsden Hospital. He is currently responsible for developing, multifunctional magnetic resonance and functional computer tomography imaging studies in cancer patients. Additional research interests are localized magnetic resonance correlation spectroscopy studies in cancer patients.

Dr. Collins is a member of several institutions, the International Society of Magnetic Resonance in Medicine, Institute of Physics, and the British Institute of Radiology.

Ian R. Young is a Senior Research Fellow with the Department of Electrical and Electronic Engineering, Imperial College London, after many years working on MRI at Hammersmith Hospital, London.

Dr. Young is a Fellow of the Royal Society and a Fellow of the Royal Academy of Engineering.